

Checking the dark matter origin of 3.53 keV line with the Milky Way center

A. Boyarsky¹, J. Franse^{1,2}, D. Iakubovskiy³, and O. Ruchayskiy⁴

¹Instituut-Lorentz for Theoretical Physics, Universiteit Leiden, Niels Bohrweg 2, Leiden, The Netherlands

²Leiden Observatory, Leiden University, Niels Bohrweg 2, Leiden, The Netherlands

³Bogolyubov Institute of Theoretical Physics, Metrologichna Str. 14-b, 03680, Kyiv, Ukraine

⁴Ecole Polytechnique Fédérale de Lausanne, FSB/ITP/LPPC, BSP, CH-1015, Lausanne, Switzerland

(■Dated: October 5, 2015)

We detect a line at 3.539 ± 0.011 keV in the deep exposure dataset of the Galactic Center region, observed with the XMM-Newton. The dark matter interpretation of the signal observed in the Perseus galaxy cluster, the Andromeda galaxy [1] and in the stacked spectra of galaxy clusters [2], together with non-observation of the line in blank sky data, put both lower and upper limits on the possible intensity of the line in the Galactic Center data. Our result is consistent with these constraints for a class of Milky Way mass models, presented previously by observers, and would correspond to radiative decay dark matter lifetime $\tau_{\text{DM}} \sim 6 - 8 \times 10^{27}$ sec. Although it is hard to exclude an astrophysical origin of this line based the Galactic Center data alone, this is an important consistency check of the hypothesis that encourages to check it with more observational data that are expected by the end of 2015.

Recently, two independent groups [1, 2] reported a detection of an unidentified X-ray line at energy 3.53 keV in the long-exposure X-ray observations of a number of dark matter-dominated objects. The authors of [2] have observed this line in a stacked XMM spectrum of 73 galaxy clusters spanning a redshift range 0.01 – 0.35 and separately in subsamples of nearby and remote clusters. Ref. [1] have found this line in the outskirts of the Perseus cluster and in the central 14' of the Andromeda galaxy. The global significance of detection of the same line in the datasets of Ref. [1] is 4.3σ (taking into account the trial factors); the signal in [2] has significance above 4σ based on completely independent data.

The position of the line is correctly redshifted between galaxy clusters [2] and between the Perseus cluster and the Andromeda galaxy [1]. In a very long exposure blank sky observation (15.7 Msec of cleaned data) the feature is absent [1]. This makes it unlikely that an instrumental effect is at the origin of this feature (e.g. an unmodeled wiggle in the effective area).

To identify this spectral feature with an atomic line in galaxy clusters, one should assume a strongly super-solar abundance of potassium or some anomalous argon transition [2]. Moreover, according to the results of [1] this should be true not only in the center of the Perseus cluster considered in [2], but also (i) in its outer parts up to at least 1/2 of its virial radius and (ii) in the Andromeda galaxy.

This result triggered significant interest as it seems consistent with a long-sought-for signal from dark matter decay [3–47], annihilation [11, 35, 48], de-excitation [11, 49–58] or conversion in the magnetic field [59–61]. Many particle physics models that predict such properties for the dark matter particle, have been put forward, including sterile neutrino, axion, axino, gravitino and many others, see for reviews e.g. [37, 62] and references therein. If the interaction of dark matter parti-

cles is weak enough (e.g. much weaker than that of the Standard Model neutrino), they need not to be stable as their lifetime can exceed the age of the Universe. Nevertheless huge amounts of dark matter particles can make the signal strong enough to be detectable even from such rare decays.

The omni-presence of dark matter in galaxies and galaxy clusters opens the way to check the decaying dark matter hypothesis [63]. The decaying dark matter signal is proportional to the *column density* $\mathcal{S}_{\text{DM}} = \int \rho_{\text{DM}} d\ell$ – the integral along the line of sight of the DM density distribution (unlike the case of annihilating dark matter, where the signal is proportional to $\int \rho_{\text{DM}}^2 d\ell$). As long as the angular size of an object is larger than the field-of-view, the distance to the object drops out which means that distant objects can give fluxes comparable to those of nearby ones [64, 65]. It also does not decrease with the distance from the centres of objects as fast as e.g. in the case of annihilating DM where the expected signal is concentrated towards the centers of DM-dominated objects. This in principle allows one to check the dark matter origin of a signal by comparison between objects and/or by studying the angular dependence of the signal within one object, rather than trying to exclude all possible astrophysical explanations for each target [66–69].

Clearly, after years of systematic searches for this signal (Ref. [66, 70–95]; see Fig. 4 in [1]) any candidate line can be detected only at the edge of the possible sensitivity of the method. Therefore, to cross-check the signal one needs long-exposure data. Moreover, even a factor 2 uncertainty in the expected signal (which is impossible to avoid) can result in the necessity to have significantly more statistics than in the initial data set in which the candidate signal was found.

So far the DM interpretation of the signal of [2] and [1] is consistent with the data: it has the correct scaling between

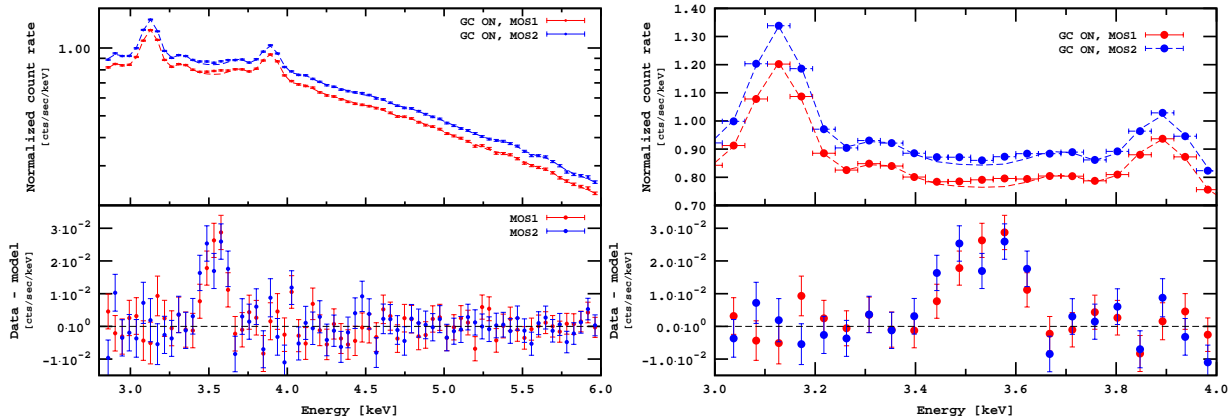


FIG. 1: *Left*: Folded count rate for MOS1 (lower curve, red) and MOS2 (upper curve, blue) and residuals (bottom) when the line at 3.54 keV is *not added*. The difference between the cameras is due to detector gaps and bad pixels. *Right*: Zoom at the range 3.0–4.0 keV.

the Perseus cluster, Andromeda and the upper bound from the non-detection in the blank sky data [1], and between different subsamples of clusters [2]. The mass and lifetime of the dark matter particle that is implied by the DM interpretation of the results of [1], is consistent with the results of [2]. The signal has radial surface brightness profiles in the Perseus cluster and Andromeda [1] that are consistent with a dark matter distribution. Although the significance of this result is not sufficient to confirm the hypothesis, they can be considered as successful sanity checks. More results are clearly needed to perform a convincing checking program as described above.

A classical target for DM searches is the centre of our Galaxy. Due to its proximity it is possible to concentrate on the very central part and therefore, even for decaying DM, one can expect a significant gain in the signal if the DM distribution in the Milky Way happens to be steeper than a cored profile. The Galactic Center (GC) region has been extensively studied by the XMM and several mega-seconds of raw exposure exist. On the other hand, the GC region has strong X-ray emission as many complicated processes occur there [96–104]. In particular, the X-ray emitting gas may contain several thermal components with different temperatures; it may be more difficult to constrain the abundances of potassium and argon reliably than in the case of intercluster medium. Therefore the GC data alone would hardly provide a convincing detection of the DM signal, as even a relatively strong candidate line could be explained by astrophysical processes. In this paper we pose a different question: *Are the observations of the Galactic Center consistent with the dark matter interpretation of the 3.53 keV line of [1, 2]?*

The DM interpretation of the 3.53 keV line in M31 and Perseus provides a prediction of the *minimal* expected flux from the GC. On the other hand, the non-detection of any signal in the off-center observations of the Milky Way halo (the blank sky dataset of [1]) provides the prediction of the *maximal* possible flux in the GC, given observational constraints on the DM distribution in the Galaxy. Therefore, even with all

the uncertainties on the DM content of the involved objects, the expected signal from the GC is bounded from both sides and provides a non-trivial check for the DM interpretation of the 3.53 keV line.

We use XMM-Newton observations of the central 14′ of the Galactic Center region with a total cleaned exposure of 1.4 Msec. We find that the spectrum has a $\sim 5.7\sigma$ line-like excess at the expected energy. The simultaneous fitting of the GC, Perseus and M31 provides a $\sim 6.7\sigma$ significant signal at the same position, with the detected fluxes being consistent with the DM interpretation. The fluxes are also consistent with the non-observation of the signal in the blank-sky and M31 off-center datasets, if one assumes a steeper-than-cored DM profile (for example, the NFW profile of Ref. [105]).

Below we summarize the details of our data analysis and discuss the results.

Data reduction. We use all archival data of the Galactic Center obtained by the EPIC MOS cameras [106] with Sgr A* less than 0.5′ from the telescope axis (see SOM, Table I). The data are reduced by the standard SAS¹ pipeline, including screening for the time-variable soft proton flares by `espfilt`. We removed the observations taken during the period MJD 54000–54500 due to strong flaring activity of Sgr A* (see SOM, Fig. 1). The data reduction and preparation of the final spectra are similar to [1]. For each reduced observation we select a circle of radius 14′ around Sgr A* and combine these spectra using the FTOOLS [107] procedure `addspec`.

Spectral modeling. To account for the cosmic-ray induced instrumental background we have subtracted the latest closed filter datasets (exposure: 1.30 Msec for MOS1 and 1.34 Msec for MOS2) [108]. The rescaling of the closed filter data has been performed such that the flux at energies $E > 10$ keV

¹ v.13.5.0 <http://xmm.esa.int/sas>

reduces to zero (see [109] for details). We model the resulting physical spectrum in the energy range 2.8–6.0 keV. The X-ray emission from the inner part of the Galactic Center contains both thermal and non-thermal components [98, 99]. Therefore, we chose to model the spectrum with a thermal plasma model (`vappec`) and a non-thermal powerlaw component modified by the `phabs` model to account for the Galactic absorption.² We set the abundances of all elements – except for Fe – to zero but model the known astrophysical lines with `gaussians` [1, 2, 111]. We selected the $\geq 2\sigma$ lines from the set of astrophysical lines of [2, 104]³. The intensities of the lines are allowed to vary, as are the central energies to account for uncertainties in detector gain and limited spectral resolution. We keep the same position of the lines between the two cameras.

The spectrum is binned to 45 eV to have about 4 bins per resolution element. The fit quality for the dataset is $\chi^2 = 108/100$ d.o.f. The resulting values for the main continuum components – the folded powerlaw index (for the integrated point source contribution), the temperature of the `vappec` model (~ 8 keV), and the absorption column density – agree well with previous studies [98, 99].

Results. The resulting spectra of the inner 14' of the Galactic Center show a $\sim 5.7\sigma$ line-like excess at 3.539 ± 0.011 keV with a flux of $(29 \pm 5) \times 10^{-6}$ cts/sec/cm² (see Fig. 1). It should be stressed that these 1σ error-bars are obtained with the `xspec` command `error` (see **Discussion** below). The position of the excess is very close to the similar excesses recently observed in Andromeda (3.53 ± 0.03 keV) and Perseus (3.50 ± 0.04 keV) reported in [1], and is less than 2σ away from the one described in [2].

We also performed combined fits of the GC dataset with those of M31 and Perseus from [1]. As mentioned, the data reduction and modeling were performed very similarly, so we suffice with repeating that the inner part of M31 is covered by almost 1 Msec of cleaned MOS exposure, whereas a little over 500 ksec of clean MOS exposure was available for Perseus (see [1] for details).

We first perform a joint fit to the Galactic Center and M31, and subsequently to the Galactic Center, M31 and Perseus. In both cases, we start with the best-fit models of each individual analysis without any lines at 3.53 keV, and then add an additional gaussian to each model, allowing the energy to vary while keeping the same position between the models. The normalizations of this line for each dataset are allowed to vary independently. In this way, the addition of the line to the combination of Galactic Center, M31 and Perseus gives 4 extra degrees of freedom, which brings the joint significance

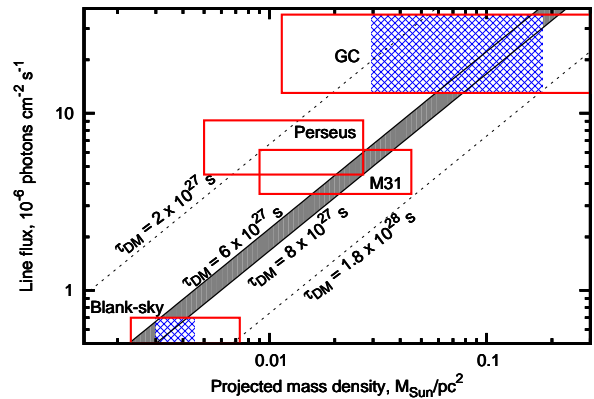


FIG. 2: The flux of the 3.53 keV line in the spectra of the GC (this work), the Perseus cluster outskirts, M31, and the blank sky [1] as a function of the DM projected mass. Diagonal lines show the expected behaviour of a decaying DM signal for a given DM particle lifetime. The vertical sizes of the boxes are $\pm 1\sigma$ statistical error on the line’s flux – or the 2σ upper bound for the blank-sky dataset. The horizontal sizes of the boxes bracket the *scatter* in the literature mass modeling (see text and Appendix A). The Milky Way halo contribution is included for M31 but not for Perseus, where it would be redshifted. The projected mass density for the GC and the Milky Way outskirts (blank sky) are correlated. The blue shaded regions show a particular NFW profile of the Milky Way [112], its horizontal size indicates uncertainties in galactic disk modeling. Other *cuspy* profiles are consistent with these flux ratios as well (c.f. [113]). The lifetime $\tau_{DM} \sim (6 - 8) \times 10^{27}$ sec is consistent with all datasets.

to $\sim 6.7\sigma$.

To further investigate possible systematic errors on the line parameters we took into account that the `gaussian` component at 3.685 keV may describe not a single line, but a complex of lines (SOM, Table II). Using the `steppar` command we scanned over the two-dimensional grid of this `gaussian`’s intrinsic width and the normalization of the line at 3.539 keV. We were able to find a new best fit with the 3.685 keV `gaussian` width being as large as 66 ± 15 eV. In this new minimum our line shifts to 3.50 ± 0.02 keV (as some of the photons were attributed to the 3.685 keV `gaussian`) and has a flux of 24×10^{-6} cts/sec/cm² with a 1σ confidence interval of $(13 - 36) \times 10^{-6}$ cts/sec/cm². The significance of the line is $\Delta\chi^2 = 9.5$ (2.6σ for 2 d.o.f.). Although the width in the new minimum seems to be too large even for the whole complex of Ar XVII lines (see **Discussion**), we treat this change of line parameters as the estimate of systematic uncertainties. To reduce these systematics one has either to resolve or to reliably model a line complex around 3.685 keV instead of representing it as one wide `gaussian` component.

As was argued in [1], an interpretation of the signal as an unmodelled wiggle in the effective area is not favoured because it should have produced a very significant signal in the blank-sky dataset as well. This is because an effect like this would produce a line-like residual proportional to the contin-

² The `Xspec` [110] v.12.8.0 is used for the spectral analysis.

³ Unlike [2] we do not include K XVIII lines at 3.47 and 3.51 keV to our model. See the discussion below

uum level. In addition, the line would not be redshifted properly for Perseus [1] and the cluster stack from [2].

Discussion. The intensity of DM decay signal should correlate with DM content of the probed objects. In order to check this we took DM distributions for Perseus, M31 and the MW from Refs. [105, 112, 114–123] (see Appendix for details) and plotted the line intensity vs. mass in the field-of-view divided by the distance squared (*projected DM density*), Fig. 2. We see that *decaying DM with a lifetime $\tau_{\text{DM}} \sim 6 - 8 \times 10^{27}$ sec would explain the signals from the GC, Perseus and M31 and the non-observation in the blank-sky dataset.* A considerable spread of projected DM masses is due to scatter between the distributions in the literature. For the GC the estimates are based on extrapolations, as there are no measurements of the DM distribution within the inner few kpc. The correlation between the GC and blank-sky projected DM densities is necessary, since these are different parts of the same halo. From comparing our GC signal with the blank-sky upper limit we see that *this requires cuspy (rather than cored) density profile of the Milky Way.* Fig. 2 shows an example of a profile consistent with both the GC detection and blank-sky upper limit, Ref. [112].

M31 and Milky Way are expected to have similar distributions, providing another consistency check. Ref. [1] showed that in order to explain the signal from central $14'$ and non-observation from M31 outskirts, the Andromeda DM density profile should be cuspy, as predicted also for the Milky Way. Fig. 2 shows that indeed large projected DM mass (i.e. cuspy profile) is preferred for M31.

Finally the Perseus signal of [1] comes from the cluster outskirts where the hydrostatic mass [121] may be underestimated [124]. This would only improve the consistency between the data sets.

The comparison of expected DM signal from GC vs. blank-sky vs. Andromeda has been investigated in simulations [113], where various realisation of the galactic DM halos were considered and high probability of finding observed flux ratios between GC and M31 and between GC and blank-sky upper limit was found.

The non-detection of the signal in stacked dSphs by [125] rules out the central values of the decay lifetime from [2] but is consistent with [1] in case of large project DM mass (also preferred from comparison with other signals, Fig. 2). The signal was not detected in stacked galaxy spectra [126]. However, a novel method of [126] has pronounced systematic effects (see Appendix B of [126]) and is the least sensitive exactly at energies $E \sim 3.5$ keV. Ref. [62] used a stacked dataset of nearby galaxies from [127] and showed that systematic effects and uncertainty in dark matter distributions [64] lead to the bound $\tau_{\text{DM}} \gtrsim 3.5 \times 10^{27}$ sec, consistent with our findings. Other bounds on decaying dark matter in the ~ 3.5 keV energy range (see [95, 127, 128] and references therein) are also consistent with our detections for lifetimes that we discuss in

this paper.

As mentioned in the **Results**, there is a degeneracy between the width of the Ar XVII complex around 3.685 keV and the normalization of the line in question. If we allow the width of the Ar XVII line to vary freely we can decrease the significance of the line at 3.539 keV to about 2σ . However, in this case the width of the gaussian at 3.685 keV should be 95 – 130 eV, which is significantly larger than we obtain when simulating a complex of four Ar XVII lines. In addition, in this case the total flux of the line at 3.685 keV becomes *higher* than the fluxes in the lines at 3.130 and 3.895 in contradiction with the atomic data (SOM, Table II).

Another way to decrease the significance of the line at 3.539 is to assume the presence of a potassium ion (K XVIII) with a line at 3.515 keV and a smaller line at 3.47 keV. If one considers the abundance of potassium as a completely free parameter (c.f. [111, 129, 130]), one can find an acceptable fit of the XMM GC data without an additional line at 3.539 keV. As described in Appendix B, due to the complicated internal temperature and abundance structures it is not possible to reliably constrain the overall potassium abundance of the GC to a degree that rules out the K XVIII origin of the 3.539 keV line *in this dataset.*

However, if we are to explain the presence of this line in the spectra by the presence of K XVIII, we have to build a model that consistently explains the fluxes in this line in different astronomical environments: in galaxy clusters (in particular Perseus) at all off-center distances from the central regions [2] to the cluster outskirts up to the virial radius [1]; in the central part of M31; and in the Galactic Center. In addition, we need to explain that this line is not observed – and therefore that this transition *should not* be excited – in the outskirts of the Milky Way and of M31 [1]. Such a consistent model does not look convincing. In particular, in M31 spectrum there are no strong astrophysical lines in 3 – 4 keV range [131]. The powerlaw continuum is well determined by fitting the data over a wider range of energies (from 2 to 8 keV) and allows a clear detection of the line at 3.53 ± 0.03 keV with $\Delta\chi^2 = 13$ [1, 131], which is also the largest line-like feature in the entire 3–4 keV range. Were this signal in M31 due to K XVIII, there should be plenty of stronger emission lines present. In addition, the authors of [2] conclude that strongly super-solar abundances of K XVIII are required to explain the observed excess of this line in their stacked cluster analysis.

In conclusion, although it is hard to exclude completely an astrophysical origin of the 3.539 keV line in the GC (due to the complicated nature of this object), the detection of this line in this object is an essential cross-check for the DM interpretation of the signal observed in Perseus and M31 [1] and in the stacked spectra of galaxy clusters [2]. A non-detection in the GC or a detection with high flux would have immediately ruled out this interpretation. As it is, the GC data rather supports DM interpretation as the line is not only observed at the same energy, but also its flux is consistent with the expectations about the DM distributions.

To settle this question, measurements with higher spectral resolution, an independent measurement of the relative abundances of elements in the GC region, and analyses of additional deep exposure datasets of DM-dominated objects are needed [113, 128, 132–135] with Astro-H [136] or future mission, Athena [137].

Acknowledgments. The work of D. I. was supported by

part by the Swiss National Science Foundation grant SCOPE IZ7370-152581, the Program of Cosmic Research of the National Academy of Sciences of Ukraine, the State Programme of Implementation of Grid Technology in Ukraine and the grant of President of Ukraine for young scientists. The work of J. F. was supported by the De Sitter program at Leiden University with funds from NWO. This research is part of the “Fundamentals of Science” program at Leiden University.

-
- [1] A. Boyarsky, O. Ruchayskiy, D. Iakubovskiy, and J. Franse, ArXiv e-prints (2014), 1402.4119.
- [2] E. Bulbul, M. Markevitch, A. Foster, R. K. Smith, M. Loewenstein, and S. W. Randall, *ApJ* **789**, 13 (2014), 1402.2301.
- [3] H. Ishida, K. S. Jeong, and F. Takahashi, *Physics Letters B* **732**, 196 (2014), 1402.5837.
- [4] T. Higaki, K. S. Jeong, and F. Takahashi, *Physics Letters B* **733**, 25 (2014), 1402.6965.
- [5] J. Jaeckel, J. Redondo, and A. Ringwald, *Phys. Rev. D* **89**, 103511 (2014), 1402.7335.
- [6] M. Czerny, T. Higaki, and F. Takahashi, *Journal of High Energy Physics* **5**, 144 (2014), 1403.0410.
- [7] H. M. Lee, S. C. Park, and W.-I. Park, ArXiv e-prints (2014), 1403.0865.
- [8] K. N. Abazajian, *Physical Review Letters* **112**, 161303 (2014), 1403.0954.
- [9] R. Krall, M. Reece, and T. Roxlo, ArXiv e-prints (2014), 1403.1240.
- [10] C. El Aisati, T. Hambye, and T. Scarna, ArXiv e-prints (2014), 1403.1280.
- [11] M. T. Frandsen, F. Sannino, I. M. Shoemaker, and O. Svendsen, *JCAP* **5**, 033 (2014), 1403.1570.
- [12] K. Hamaguchi, M. Ibe, T. T. Yanagida, and N. Yokozaki, ArXiv e-prints (2014), 1403.1398.
- [13] K. Kong, J.-C. Park, and S. C. Park, ArXiv e-prints (2014), 1403.1536.
- [14] S. Baek and H. Okada, ArXiv e-prints (2014), 1403.1710.
- [15] K. Nakayama, F. Takahashi, and T. T. Yanagida, ArXiv e-prints (2014), 1403.1733.
- [16] K.-Y. Choi and O. Seto, ArXiv e-prints (2014), 1403.1782.
- [17] B. Shuve and I. Yavin, *Phys. Rev. D* **89**, 113004 (2014), 1403.2727.
- [18] C. Kolda and J. Unwin, ArXiv e-prints (2014), 1403.5580.
- [19] R. Allahverdi, B. Dutta, and Y. Gao, ArXiv e-prints (2014), 1403.5717.
- [20] A. G. Dias, A. C. B. Machado, C. C. Nishi, A. Ringwald, and P. Vaudrevange, *Journal of High Energy Physics* **6**, 37 (2014), 1403.5760.
- [21] N.-E. Bomark and L. Roszkowski, ArXiv e-prints (2014), 1403.6503.
- [22] S. Pei Liew, *JCAP* **5**, 044 (2014), 1403.6621.
- [23] K. Nakayama, F. Takahashi, and T. T. Yanagida, *Physics Letters B* **734**, 178 (2014), 1403.7390.
- [24] Z. Kang, P. Ko, T. Li, and Y. Liu, ArXiv e-prints (2014), 1403.7742.
- [25] H. Okada, ArXiv e-prints (2014), 1404.0280.
- [26] S. V. Demidov and D. S. Gorbunov, ArXiv e-prints (2014), 1404.1339.
- [27] F. S. Queiroz and K. Sinha, *Physics Letters B* **735**, 69 (2014), 1404.1400.
- [28] K. S. Babu and R. N. Mohapatra, *Phys. Rev. D* **89**, 115011 (2014), 1404.2220.
- [29] K. Prasad Modak, ArXiv e-prints (2014), 1404.3676.
- [30] J. L. Rosner, ArXiv e-prints (2014), 1404.5198.
- [31] J. Barry, J. Heeck, and W. Rodejohann, ArXiv e-prints (2014), 1404.5955.
- [32] D. J. Robinson and Y. Tsai, ArXiv e-prints (2014), 1404.7118.
- [33] J. Kubo, K. Sham Lim, and M. Lindner, ArXiv e-prints (2014), 1405.1052.
- [34] M. Drewes, ArXiv e-prints (2014), 1405.2931.
- [35] S. Baek, P. Ko, and W.-I. Park, ArXiv e-prints (2014), 1405.3730.
- [36] K. Nakayama, F. Takahashi, and T. T. Yanagida, ArXiv e-prints (2014), 1405.4670.
- [37] J. Bateman, I. McHardy, A. Merle, T. R. Morris, and H. Ulbricht, ArXiv e-prints (2014), 1405.5536.
- [38] S. Chakraborty, D. K. Ghosh, and S. Roy, ArXiv e-prints (2014), 1405.6967.
- [39] M. Lattanzi, R. A. Lineros, and M. Taoso, ArXiv e-prints (2014), 1406.0004.
- [40] M. Kawasaki, N. Kitajima, and F. Takahashi, ArXiv e-prints (2014), 1406.0660.
- [41] N. Chen, Z. Liu, and P. Nath, ArXiv e-prints (2014), 1406.0687.
- [42] H. Ishida and H. Okada, ArXiv e-prints (2014), 1406.5808.
- [43] A. Abada, G. Arcadi, and M. Lucente, ArXiv e-prints (2014), 1406.6556.
- [44] A. Abada, V. De Romeri, and A. M. Teixeira, ArXiv e-prints (2014), 1406.6978.
- [45] H. Baer, K.-Y. Choi, J. E. Kim, and L. Roszkowski, ArXiv e-prints (2014), 1407.0017.
- [46] A. Ringwald, ArXiv e-prints (2014), 1407.0546.
- [47] B. Dutta, I. Gogoladze, R. Khalid, and Q. Shafi, ArXiv e-prints (2014), 1407.0863.
- [48] E. Dudas, L. Heurtier, and Y. Mambrini, ArXiv e-prints (2014), 1404.1927.
- [49] D. P. Finkbeiner and N. Weiner, ArXiv e-prints (2014), 1402.6671.
- [50] J. M. Cline, Z. Liu, G. D. Moore, Y. Farzan, and W. Xue, *Phys. Rev. D* **89**, 121302 (2014), 1404.3729.
- [51] C.-W. Chiang and T. Yamada, ArXiv e-prints (2014), 1407.0460.
- [52] C.-Q. Geng, D. Huang, and L.-H. Tsai, ArXiv e-prints (2014), 1406.6481.

- [53] H. Okada and T. Toma, ArXiv e-prints (2014), 1404.4795.
- [54] H. M. Lee, ArXiv e-prints (2014), 1404.5446.
- [55] A. Falkowski, Y. Hochberg, and J. T. Ruderman, *Journal of High Energy Physics* **11**, 140 (2014), 1409.2872.
- [56] J. M. Cline and A. R. Frey, *JCAP* **10**, 013 (2014), 1408.0233.
- [57] K. K. Boddy, J. L. Feng, M. Kaplinghat, Y. Shadmi, and T. M. P. Tait, *Phys. Rev. D* **90**, 095016 (2014), 1408.6532.
- [58] Y. Mambrini and T. Toma, ArXiv e-prints (2015), 1506.02032.
- [59] J. P. Conlon and A. J. Powell, ArXiv e-prints (2014), 1406.5518.
- [60] M. Cicoli, J. P. Conlon, M. C. D. Marsh, and M. Rummel, ArXiv e-prints (2014), 1403.2370.
- [61] J. P. Conlon and F. V. Day, ArXiv e-prints (2014), 1404.7741.
- [62] D. A. Iakubovskiy, *Advances in Astronomy and Space Physics* **4**, 9 (2014), 1410.2852.
- [63] A. Boyarsky, O. Ruchayskiy, M. G. Walker, S. Riemeer-Sørensen, and S. H. Hansen, *MNRAS* **407**, 1188 (2010), 1001.0644.
- [64] A. Boyarsky, A. Neronov, O. Ruchayskiy, and I. Tkachev, *Phys. Rev. Lett.* **104**, 191301 (2010), 0911.3396.
- [65] A. Boyarsky, O. Ruchayskiy, D. Iakubovskiy, A. V. Maccio', and D. Malyshev (2009), 0911.1774.
- [66] A. Boyarsky, A. Neronov, O. Ruchayskiy, M. Shaposhnikov, and I. Tkachev, *Phys. Rev. Lett.* **97**, 261302 (2006), astro-ph/0603660.
- [67] A. Boyarsky, J. W. den Herder, O. Ruchayskiy, et al. (2009), a white paper submitted in response to the Fundamental Physics Roadmap Advisory Team (FPR-AT) Call for White Papers, 0906.1788.
- [68] K. N. Abazajian (2009), white paper submitted to the Astro 2010 Decadal Survey, *Cosmology and Fundamental Physics Science*, 0903.2040.
- [69] A. Boyarsky, D. Iakubovskiy, and O. Ruchayskiy, *Phys. Dark Univ.* **1**, 136 (2012), 1306.4954.
- [70] K. Abazajian, G. M. Fuller, and W. H. Tucker, *Astrophys. J.* **562**, 593 (2001), astro-ph/0106002.
- [71] A. D. Dolgov and S. H. Hansen, *Astropart. Phys.* **16**, 339 (2002), hep-ph/0009083.
- [72] A. Boyarsky, A. Neronov, O. Ruchayskiy, and M. Shaposhnikov, *MNRAS* **370**, 213 (2006), astro-ph/0512509.
- [73] A. Boyarsky, A. Neronov, O. Ruchayskiy, and M. Shaposhnikov, *Phys. Rev. D* **74**, 103506 (2006), astro-ph/0603368.
- [74] S. Riemeer-Sørensen, S. H. Hansen, and K. Pedersen, *ApJ* **644**, L33 (2006), arXiv:astro-ph/0603661.
- [75] C. R. Watson, J. F. Beacom, H. Yuksel, and T. P. Walker, *Phys. Rev. D* **74**, 033009 (2006), astro-ph/0605424.
- [76] S. Riemeer-Sørensen, K. Pedersen, S. H. Hansen, and H. Dahle, *Phys. Rev. D* **76**, 043524 (2007), arXiv:astro-ph/0610034.
- [77] A. Boyarsky, J. Nevalainen, and O. Ruchayskiy, *A&A* **471**, 51 (2007), astro-ph/0610961.
- [78] K. Abazajian and S. M. Koushiappas, *Phys. Rev. D* **74**, 023527 (2006), astro-ph/0605271.
- [79] A. Boyarsky, O. Ruchayskiy, and M. Markevitch, *ApJ* **673**, 752 (2008), astro-ph/0611168.
- [80] A. Boyarsky, J. W. den Herder, A. Neronov, and O. Ruchayskiy, *Astropart. Phys.* **28**, 303 (2007), astro-ph/0612219.
- [81] H. Yuksel, J. F. Beacom, and C. R. Watson, *Phys. Rev. Lett.* **101**, 121301 (2008), 0706.4084.
- [82] A. Boyarsky, D. Iakubovskiy, O. Ruchayskiy, and V. Savchenko, *MNRAS* **387**, 1361 (2008), arXiv:0709.2301.
- [83] A. Boyarsky, D. Malyshev, A. Neronov, and O. Ruchayskiy, *MNRAS* **387**, 1345 (2008), 0710.4922.
- [84] M. Loewenstein, A. Kusenko, and P. L. Biermann, *ApJ* **700**, 426 (2009), 0812.2710.
- [85] S. Riemeer-Sørensen and S. H. Hansen, *A&A* **500**, L37 (2009).
- [86] M. Loewenstein and A. Kusenko, *Astrophys. J.* **714**, 652 (2010), 0912.0552.
- [87] A. Boyarsky, O. Ruchayskiy, D. Iakubovskiy, M. G. Walker, S. Riemeer-Sørensen, and S. H. Hansen, *MNRAS* **407**, 1188 (2010), 1001.0644.
- [88] N. Mirabal and D. Nieto, ArXiv e-prints (2010), 1003.3745.
- [89] N. Mirabal, *MNRAS* **409**, L128 (2010), 1010.4706.
- [90] D. A. Prokhorov and J. Silk (2010), 1001.0215.
- [91] E. Borriello, M. Paolillo, G. Miele, G. Longo, and R. Owen, *Mon. Not. Roy. Astron. Soc.* **425**, 1628 (2012), 1109.5943.
- [92] C. R. Watson, Z. Li, and N. K. Polley, *JCAP* **3**, 18 (2012), 1111.4217.
- [93] M. Loewenstein and A. Kusenko, *Astrophys. J.* **751**, 82 (2012), 1203.5229.
- [94] A. Kusenko, M. Loewenstein, and T. T. Yanagida, ArXiv e-prints (2012), 1209.6403.
- [95] S. Horiuchi, P. J. Humphrey, J. Onorbe, K. N. Abazajian, M. Kaplinghat, et al., *Phys. Rev. D* **89**, 025017 (2013), 1311.0282.
- [96] K. Koyama, H. Awaki, H. Kunieda, S. Takano, and Y. Tawara, *Nature* **339**, 603 (1989).
- [97] K. Koyama, Y. Maeda, T. Sonobe, T. Takeshima, Y. Tanaka, and S. Yamauchi, *PASJ* **48**, 249 (1996).
- [98] H. Kaneda, K. Makishima, S. Yamauchi, K. Koyama, K. Matsuzaki, and N. Y. Yamasaki, *ApJ* **491**, 638 (1997).
- [99] M. P. Muno, J. S. Arabadjis, F. K. Baganoff, M. W. Bautz, W. N. Brandt, P. S. Broos, E. D. Feigelson, G. P. Garmire, M. R. Morris, and G. R. Ricker, *ApJ* **613**, 1179 (2004), astro-ph/0403463.
- [100] K. Koyama, Y. Hyodo, T. Inui, H. Nakajima, H. Matsumoto, T. G. Tsuru, T. Takahashi, Y. Maeda, N. Y. Yamazaki, H. Murakami, et al., *PASJ* **59**, 245 (2007), astro-ph/0609215.
- [101] M. P. Muno, F. K. Baganoff, W. N. Brandt, S. Park, and M. R. Morris, *ApJ* **656**, L69 (2007), astro-ph/0611651.
- [102] M. Revnivtsev, S. Sazonov, E. Churazov, W. Forman, A. Vikhlinin, and R. Sunyaev, *Nature* **458**, 1142 (2009), 0904.4649.
- [103] G. Ponti, R. Terrier, A. Goldwurm, G. Belanger, and G. Trap, *ApJ* **714**, 732 (2010), 1003.2001.
- [104] H. Uchiyama, M. Nobukawa, T. G. Tsuru, and K. Koyama, *PASJ* **65**, 19 (2013), 1209.0067.
- [105] M. Weber and W. de Boer, *A&A* **509**, A25 (2010), 0910.4272.
- [106] M. J. L. Turner, A. Abbey, M. Arnaud, M. Balasini, M. Barbera, E. Belsole, P. J. Bennie, J. P. Bernard, G. F. Bignami, M. Boer, et al., *A&A* **365**, L27 (2001), arXiv:astro-ph/0011498.
- [107] Irby, B., The ftools webpage, HeaSoft, http://heasarc.gsfc.nasa.gov/docs/software/ftools/ftools_menu.html (2008).
- [108] *Repository of xmm-newton epic filter wheel closed data*, http://xmm2.esac.esa.int/external/xmm_sw_cal/backgr
- [109] J. Nevalainen, M. Markevitch, and D. Lumb, *ApJ* **629**, 172 (2005), astro-ph/0504362.
- [110] K. A. Arnaud, in *Astronomical Data Analysis Software and Systems V*, edited by G. H. Jacoby and J. Barnes (San Francisco, ASP, 1996), vol. 101 of *A.S.P. Conference Serie*, p. 17.
- [111] S. Riemeer-Sørensen, ArXiv e-prints (2014), 1405.7943.
- [112] M. C. Smith et al., *Mon. Not. Roy. Astron. Soc.* **379**, 755 (2007), astro-ph/0611671.
- [113] M. R. Lovell, G. Bertone, A. Boyarsky, A. Jenkins, and O. Ruchayskiy, *MNRAS* **451**, 1573 (2015), 1411.0311.

- [114] L. M. Widrow and J. Dubinski, *ApJ* **631**, 838 (2005), arXiv:astro-ph/0506177.
- [115] J. J. Geehan, M. A. Fardal, A. Babul, and P. Guhathakurta, *MNRAS* **366**, 996 (2006), arXiv:astro-ph/0501240.
- [116] G. Battaglia et al., *Mon. Not. Roy. Astron. Soc.* **364**, 433 (2005), astro-ph/0506102.
- [117] G. Battaglia, A. Helmi, H. Morrison, P. Harding, E. W. Olszewski, M. Mateo, K. C. Freeman, J. Norris, and S. A. Shectman, *MNRAS* **370**, 1055 (2006).
- [118] L. Chemin, C. Carignan, and T. Foster, *Astrophys. J.* **705**, 1395 (2009), 0909.384.
- [119] E. Corbelli, S. Lorenzoni, R. A. M. Walterbos, R. Braun, and D. A. Thilker, *A&A* **511**, A89 (2010), 0912.4133.
- [120] P. J. McMillan, *MNRAS* **414**, 2446 (2011), 1102.4340.
- [121] A. Simionescu, S. W. Allen, A. Mantz, N. Werner, Y. Takei, R. G. Morris, A. C. Fabian, J. S. Sanders, P. E. J. Nulsen, M. R. George, et al., *Science* **331**, 1576 (2011), 1102.2429.
- [122] F. Nesti and P. Salucci, *JCAP* **7**, 016 (2013), 1304.5127.
- [123] X. X. Xue et al. (SDSS), *Astrophys. J.* **684**, 1143 (2008), 0801.1232.
- [124] N. Okabe, K. Umetsu, T. Tamura, Y. Fujita, M. Takizawa, Y.-Y. Zhang, K. Matsushita, T. Hamana, Y. Fukazawa, T. Futamase, et al., ArXiv e-prints (2014), 1406.3451.
- [125] D. Malyshev, A. Neronov, and D. Eckert, *Phys. Rev. D* **90**, 103506 (2014), 1408.3531.
- [126] M. E. Anderson, E. Churazov, and J. N. Bregman, ArXiv e-prints (2014), 1408.4115.
- [127] D. Iakubovskiy, Ph.D. thesis, Instituut-Lorentz for Theoretical Physics (2013).
- [128] N. Sekiya, N. Y. Yamasaki, and K. Mitsuda, ArXiv e-prints (2015), 1504.02826.
- [129] E. Carlson, T. Jeltema, and S. Profumo, *JCAP* **2**, 009 (2015), 1411.1758.
- [130] T. E. Jeltema and S. Profumo, ArXiv e-prints (2014), 1408.1699.
- [131] A. Boyarsky, J. Franse, D. Iakubovskiy, and O. Ruchayskiy, ArXiv e-prints (2014), 1408.4388.
- [132] K. Koyama, J. Kataoka, M. Nobukawa, H. Uchiyama, S. Nakashima, F. Aharonian, M. Chernyakova, Y. Ichinohe, K. K. Nobukawa, Y. Maeda, et al., ArXiv e-prints (2014), 1412.1170.
- [133] E. Figueroa-Feliciano, A. J. Anderson, D. Castro, D. C. Goldfinger, J. Rutherford, M. E. Eckart, R. L. Kelley, C. A. Kilbourne, D. McCammon, K. Morgan, et al., ArXiv e-prints (2015), 1506.05519.
- [134] D. Iakubovskiy, ArXiv e-prints (2015), 1507.02857.
- [135] E. G. Speckhard, K. C. Y. Ng, J. F. Beacom, and R. Laha, ArXiv e-prints (2015), 1507.04744.
- [136] T. Kitayama, M. Bautz, M. Markevitch, K. Matsushita, S. Allen, M. Kawaharada, B. McNamara, N. Ota, H. Akamatsu, J. de Plaa, et al., ArXiv e-prints (2014), 1412.1176.
- [137] A. Neronov and D. Malyshev, ArXiv e-prints (2015), 1509.02758.
- [138] T. Abbey, J. Carpenter, A. Read, A. Wells, Xmm Science Centre, and Swift Mission Operations Center, in *The X-ray Universe 2005*, edited by A. Wilson (2006), vol. 604 of *ESA Special Publication*, p. 943.
- [139] *Xmm-newton epic mos1 ccd6 update*, http://xmm.esac.esa.int/external/xmm_news/items/MO
- [140] D. Porquet, N. Grosso, P. Predehl, G. Hasinger, F. Yusef-Zadeh, B. Aschenbach, G. Trap, F. Melia, R. S. Warwick, A. Goldwurm, et al., *A&A* **488**, 549 (2008), 0806.4088.
- [141] J. F. Navarro, C. S. Frenk, and S. D. M. White, *ApJ* **490**, 493 (1997), astro-ph/9611107.
- [142] A. Burkert, *ApJ* **447**, L25+ (1995), arXiv:astro-ph/9504041.
- [143] G. Gentile, P. Salucci, U. Klein, D. Vergani, and P. Kalberla, *MNRAS* **351**, 903 (2004), astro-ph/0403154.
- [144] S. M. Kent, *AJ* **91**, 1301 (1986).
- [145] B. Moore, T. Quinn, F. Governato, J. Stadel, and G. Lake, *MNRAS* **310**, 1147 (1999), astro-ph/9903164.
- [146] J. J. Binney and N. W. Evans, *MNRAS* **327**, L27 (2001), astro-ph/0108505.
- [147] A. J. Deason, V. Belokurov, N. W. Evans, and J. An, *MNRAS* **424**, L44 (2012), 1204.5189.
- [148] N. Bernal and S. Palomares-Ruiz, *JCAP* **1**, 006 (2012), 1103.2377.
- [149] Y. Sofue, M. Honma, and T. Omodaka, *PASJ* **61**, 227 (2009), 0811.0859.
- [150] C. Alcock, R. A. Allsman, T. S. Axelrod, D. P. Bennett, K. H. Cook, K. C. Freeman, K. Griest, J. A. Guern, M. J. Lehner, S. L. Marshall, et al., *ApJ* **461**, 84 (1996), arXiv:astro-ph/9506113.
- [151] M. R. Merrifield, *AJ* **103**, 1552 (1992).
- [152] F. Donato, G. Gentile, P. Salucci, C. Frigerio Martins, M. I. Wilkinson, G. Gilmore, E. K. Grebel, A. Koch, and R. Wyse, *MNRAS* **397**, 1169 (2009), 0904.4054.
- [153] G. Gentile, B. Famaey, H. Zhao, and P. Salucci, *Nature* **461**, 627 (2009), 0909.5203.
- [154] T. H. Reiprich and H. Böhringer, *ApJ* **567**, 716 (2002), astro-ph/0111285.
- [155] Y. Chen, T. H. Reiprich, H. Böhringer, Y. Ikebe, and Y.-Y. Zhang, *A&A* **466**, 805 (2007), astro-ph/0702482.
- [156] A. Simionescu, N. Werner, O. Urban, S. W. Allen, A. C. Fabian, J. S. Sanders, A. Mantz, P. E. J. Nulsen, and Y. Takei, *ApJ* **757**, 182 (2012), 1208.2990.
- [157] E. Storm, T. E. Jeltema, S. Profumo, and L. Rudnick, *Astrophys. J.* **768**, 106 (2013), 1210.0872.
- [158] S. Ettori, S. De Grandi, and S. Molendi, *A&A* **391**, 841 (2002), astro-ph/0206120.
- [159] R. Wojtak and E. L. Łokas, *MNRAS* **377**, 843 (2007), astro-ph/0606618.
- [160] A. Klypin, H. Zhao, and R. S. Somerville, *ApJ* **573**, 597 (2002), astro-ph/0110390.
- [161] M. S. Seigar, A. J. Barth, and J. S. Bullock, *MNRAS* **389**, 1911 (2008), astro-ph/0612228.
- [162] E. Tempel, A. Tamm, and P. Tenjes, **707** (2007), 0707.4374.
- [163] M. P. Muno, F. K. Baganoff, M. W. Bautz, E. D. Feigelson, G. P. Garmire, M. R. Morris, S. Park, G. R. Ricker, and L. K. Townsley, *ApJ* **613**, 326 (2004), astro-ph/0402087.
- [164] T. E. Jeltema and S. Profumo, ArXiv e-prints (2014), 1408.1699.

Supplementary material

| | ObsID | Off-center angle arcmin | Cleaned exposure MOS1/MOS2 [ksec] | FoV [arcmin ²] MOS1/MOS2 |
|----|-------------------------|----------------------------|--------------------------------------|---|
| 1 | 0111350101 | 0.017 | 40.8/40.7 | 570.5/570.3 |
| 2 | 0111350301 | 0.017 | 7.2/6.8 | 565.8/573.4 |
| 3 | 0112972101 | 0.087 | 20.8/21.4 | 571.4/572.0 |
| 4 | 0202670501 | 0.003 | 21.4/26.5 | 564.9/573.4 |
| 5 | 0202670601 | 0.003 | 29.6/31.1 | 563.8/574.1 |
| 6 | 0202670701 | 0.003 | 76.0/80.0 | 570.4/573.3 |
| 7 | 0202670801 | 0.003 | 86.9/91.0 | 569.2/572.8 |
| 8 | 0402430301 ^a | 0.002 | 57.6/60.2 | 475.8/572.1 |
| 9 | 0402430401 ^a | 0.002 | 37.3/37.8 | 476.2/572.3 |
| 10 | 0402430701 ^a | 0.002 | 23.1/25.2 | 478.5/573.1 |
| 11 | 0504940201 ^a | 0.286 | 7.7/8.5 | 487.6/572.6 |
| 12 | 0505670101 ^a | 0.002 | 65.7/73.7 | 472.0/573.2 |
| 13 | 0554750401 | 0.003 | 31.6/31.5 | 483.4/574.0 |
| 14 | 0554750501 | 0.003 | 39.6/39.2 | 487.0/574.0 |
| 15 | 0554750601 | 0.003 | 35.5/36.4 | 487.0/573.3 |
| 16 | 0604300601 | 0.003 | 28.9/30.0 | 487.1/573.1 |
| 17 | 0604300701 | 0.003 | 35.1/37.1 | 487.4/572.7 |
| 18 | 0604300801 | 0.003 | 34.9/34.2 | 487.8/572.5 |
| 19 | 0604300901 | 0.003 | 21.1/20.7 | 485.1/574.0 |
| 20 | 0604301001 | 0.003 | 35.3/38.6 | 487.4/573.6 |
| 21 | 0658600101 | 0.078 | 46.5/47.6 | 477.2/573.0 |
| 22 | 0658600201 | 0.078 | 38.3/39.7 | 478.3/572.3 |
| 23 | 0674600601 | 0.002 | 9.0/9.4 | 483.2/573.8 |
| 24 | 0674600701 | 0.003 | 12.8/13.5 | 484.9/575.0 |
| 25 | 0674600801 | 0.003 | 17.9/18.2 | 481.4/574.1 |
| 26 | 0674601001 | 0.003 | 20.0/21.5 | 480.9/573.7 |
| 27 | 0674601101 | 0.003 | 10.1/10.7 | 480.4/573.8 |

TABLE I: Properties of the XMM observations of the Galactic Center used in our analysis. We have only used observations with centers located within 0.5' around Sgr A*. The difference in FoVs between MOS1 and MOS2 cameras is due to the loss CCD6 in MOS1 camera, see [138, 139] for details.

^a Observation discarded from our analysis due to flares in Sgr a*, see Fig. 3 and [140].

Appendix A: Dark Matter Profiles of the Milky Way

The distribution of dark matter in galaxies, galaxy groups and galaxy clusters can be described by several density profiles. In this work we concentrated on four popular choices for dark matter density profiles.

I. Numerical (N-body) simulations of the cold dark matter model have shown that the dark matter distribution in all relaxed halos can be fitted with the universal Navarro-Frenk-White (NFW) profile [141]

$$\rho_{\text{NFW}}(r) = \frac{\rho_s r_s}{r(1 + r/r_s)^2} \quad (\text{A1})$$

parametrised by ρ_s and r_s .

II. The Burkert (BURK) profile [142] has been shown to be successful in explaining the kinematics of disk systems (e.g. [143]):

$$\rho_{\text{BURK}}(r) = \frac{\rho_B r_B^3}{(r_B + r)(r_B^2 + r^2)}. \quad (\text{A2})$$

III. Another common parametrizations of cored profiles are given by the pseudo-isothermal (ISO) profile [144]

$$\rho_{\text{ISO}}(r) = \frac{\rho_c}{1 + r^2/r_c^2}. \quad (\text{A3})$$

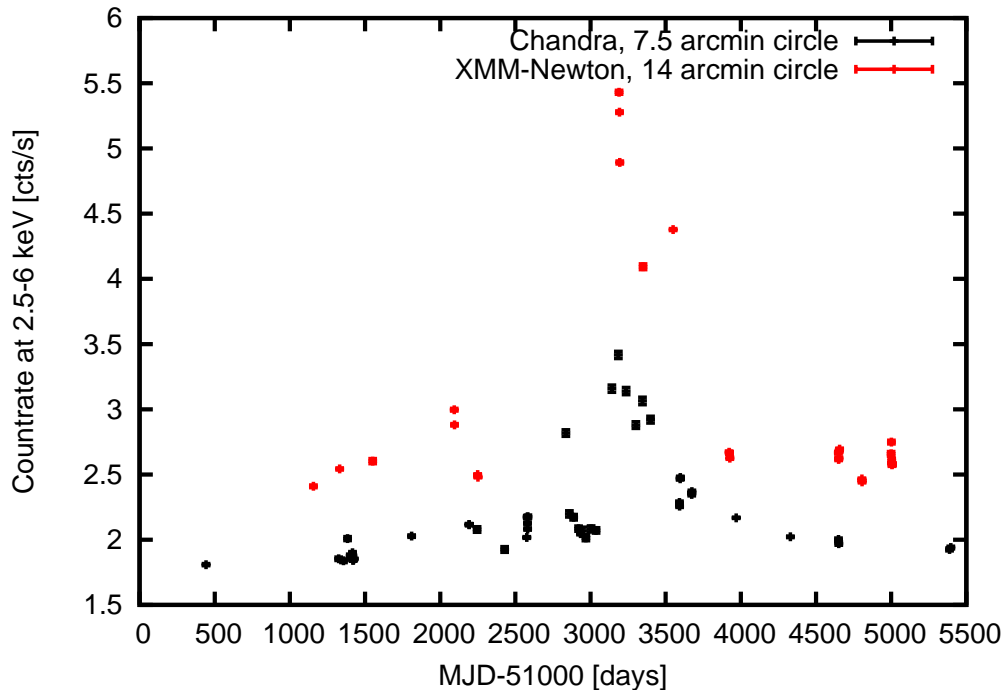


FIG. 3: Average count rates on regions centered in Sgr a* using *XMM-Newton* (red) and *Chandra* (black). The enhancement at MJD 54000-54500 are due to strong flaring activity of Sgr a*, see [140] for details. 5 *XMM-Newton* observations during this flaring period were discarded from our analysis, see Table I for details.

| Ion | Position keV | Upper level | Lower level | Emissivity ph cm ³ s ⁻¹ | T _e peak keV | Relative intensity |
|----------|-----------------|-------------|-------------|--|----------------------------|--------------------|
| Ca XIX | 3.902 | 7 | 1 | 3.913e-18 | 2.725e+0 | 0.59 |
| Ca XIX | 3.883 | 5 | 1 | 6.730e-19 | 2.725e+0 | 0.10 |
| Ca XIX | 3.861 | 2 | 1 | 1.242e-18 | 2.165e+0 | 0.19 |
| Ar XVII | 3.685 | 13 | 1 | 8.894e-19 | 1.719e+0 | 0.13 |
| Ar XVII | 3.683 | 11 | 1 | 3.729e-20 | 1.719e+0 | 0.01 |
| Ar XVII | 3.618 | 10077 | 2 | 3.627e-20 | 1.366e+0 | 0.01 |
| Ar XVII | 3.617 | 10078 | 3 | 9.355e-20 | 1.366e+0 | 0.01 |
| Ar XVIII | 3.323 | 4 | 1 | 4.052e-18 | 3.431e+0 | 0.61 |
| Ar XVIII | 3.318 | 3 | 1 | 2.061e-18 | 3.431e+0 | 0.31 |
| S XVI | 3.276 | 12 | 1 | 9.146e-19 | 2.165e+0 | 0.14 |
| Ar XVII | 3.140 | 7 | 1 | 6.604e-18 | 1.719e+0 | 1.00 |
| Ar XVII | 3.126 | 6 | 1 | 7.344e-19 | 1.719e+0 | 0.11 |
| Ar XVII | 3.124 | 5 | 1 | 1.018e-18 | 1.719e+0 | 0.15 |
| S XVI | 3.107 | 7 | 1 | 3.126e-18 | 2.165e+0 | 0.47 |
| S XVI | 3.106 | 6 | 1 | 1.584e-18 | 2.165e+0 | 0.24 |
| Ar XVII | 3.104 | 2 | 1 | 2.575e-18 | 1.719e+0 | 0.39 |
| S XV | 3.101 | 37 | 1 | 7.252e-19 | 1.366e+0 | 0.11 |
| S XV | 3.033 | 23 | 1 | 1.556e-18 | 1.366e+0 | 0.24 |

TABLE II: List of astrophysical lines at 3-4 keV expected in our model. Basic line parameters such as energy, type of ion, type of transition – are taken from AtomDB database. Only the strongest lines are shown. Close lines of the same ion are grouped with horizontal lines.

IV. The profile found by [145] from simulations is described by:

$$\rho_{\text{MOORE}}(r) = \frac{\rho_c}{\sqrt{r/r_s}(1 + \sqrt{r/r_s})} \quad (\text{A4})$$

V. [146] found a profile from lensing data of the MW with the following general shape (BE in the following):

$$\rho_{\text{BE}}(r) = \frac{\rho_c}{(r/r_s)(1 + (r/r_s))^{2.7}} \quad (\text{A5})$$

Because we reside in the inner part of Milky Way dark matter halo, it is the only object whose dark matter decay signal would be spread across the whole sky. The dark matter column density for the Milky Way halo can be calculated using the expression [77]

$$\mathcal{S}_{\text{DM}}^{\text{MW}}(\phi) = \int_0^\infty \rho_{\text{DM}}(r(z, \phi)) dz \quad (\text{A6})$$

where $r(z, \phi) = \sqrt{r_\odot^2 + z^2 - 2zr_\odot \cos \phi}$ is the distance from the galactic center with z the distance along the line of sight and ϕ the angle away from the GC for an observer at earth (itself at r_\odot from the GC). Expressed in galactic coordinates (l, b)

$$\cos \phi = \cos b \cos l. \quad (\text{A7})$$

It can be seen (e.g. [66, 77, 83]) that the function $\mathcal{S}_{\text{DM}}^{\text{MW}}$ can change only by a factor of few, when moving from the Galactic center ($\phi = 0^\circ$) to the anti-center ($\phi = 180^\circ$). That is, the Milky Way contribution to the decay is an all-sky signal.

The flux received at earth produced by dark matter decaying inside the cone of view, we can approximate by

$$F_{\text{DM}}^{\text{FoV}} = \mathcal{S}_{\text{DM}}^{\text{MW}}(\phi)\Omega\Gamma/4\pi \quad (\text{A8})$$

in photons $\text{s}^{-1} \text{cm}^{-2}$, with Ω the size of the field of view in sr , Γ the decay width and the 4π to complete the distance modulus (the distance is already included in the Ω).

The exact solution, taking into account the varying density over the field of view, is

$$F_{\text{DM}}^{\text{FoV}} = \Sigma_{\text{DM}}^{\text{FoV}}\Gamma/4\pi \quad (\text{A9})$$

$$\Sigma_{\text{DM}}^{\text{FoV}} = 2\pi \int_{\phi=0}^{\phi=\omega} \int_{z=0}^{z=\infty} \frac{\rho(r(z, \phi))}{z^2} z^2 \sin(\phi) d\phi dz \quad (\text{A10})$$

for a circular field of view centered on the GC, with a radius of ω .

The mass modeling of the Milky Way is continuously updated and improved (see e.g. [105, 112, 117, 120, 122, 123, 147–151]). In Table III we summarize recent results. We are interested in predicting the flux from dark matter decay based on the dark matter content. Therefore, using the DM distributions in the MW as reported in this table, we compute $\Sigma_{\text{DM}}^{\text{FoV}}$ for the galactic center and blank sky observations. In the galactic center case, we perform the integral in eq. A10 for $\omega = 14'$, and then correct the results for detector gaps with the ratio of the exposure-weighted average FoV size (corrected for detector gaps) to the size of an ideal $14'$ FoV. For the blank sky dataset, we computed $\mathcal{S}_{\text{DM}}^{\text{MW}}\Omega$ (see eq. A6) for each blank sky pointing (each with its own ϕ), therefore assuming that so far away from the GC the DM density does not vary appreciably over the FoV, and take the exposure and FoV weighted average of all those pointings. It is then, just like the case for the GC, corrected for detector gaps.

Regarding the mass modeling of the Galactic Center, there are additional complications. Firstly, even though according to [152, 153], the central surface densities of spiral galaxies are comparable, our field-of-view is only $14'$ in radius which translates to a physical scale of order 30 pc at the center of the halo, which is much smaller than one scale length. It is unfortunately not possible to observationally determine the DM distribution of the Milky Way within about 3 kpc from the halo center. Secondly, at these small scales, baryons dominate the mass budget and baryon physics may play an important role in shaping the DM distribution, in addition to possible warm dark matter effects. However, the extent of the influence of the processes is not well known. Thirdly, the central 3 kpc of the NFW distributions in Table III contribute between roughly 80% (least concentrated) to 90% (most concentrated) of the total $\Sigma_{\text{DM}}^{\text{FoV}}$ for the GC observations. Therefore the best we can do is extrapolate profiles measured at larger radii down to the lower radii. We remain agnostic about the very central DM distribution and assume that uncertainty is enclosed within the spread in the different types of profiles that we already examined.

Recently, [113] analysed the high-resolution Aquarius simulations specifically in order to predict dark matter decay fluxes. Milky Way and Andromeda-like halos from these simulations were selected, and the fluxes determined based on the exposure times and position angles as used in this work and in [1]. Since the flux in this case is determined solely from the mass inside

| Authors | Profile | r_\odot kpc | ρ_* $10^6 M_\odot / \text{kpc}^3$ | r_* kpc | $\Sigma_{DM,GC}^{FoV}$ $10^{-3} M_\odot / \text{pc}^2$ | $\Sigma_{DM,BS}^{FoV}$ $10^{-3} M_\odot / \text{pc}^2$ | GC/BS ratio |
|---|--------------------|------------------|---|-------------------------|---|---|------------------------|
| Smith et al. 2007 [112] ^a | NFW | 8 | $25.2^{+6.2}_{-3.8}$ | $10.6^{+0.8}_{-0.6}$ | $142.6^{+38.2}_{-20.9}$ | $5.6^{+1.3}_{-0.7}$ | $25.6^{+11.6}_{-7.8}$ |
| | NFW | 8 | $1.4^{+1.2}_{-0.5}$ | $39.6^{+4.5}_{-3.2}$ | $35.2^{+11.6}_{-5.7}$ | $3.5^{+1.0}_{-0.5}$ | $10.0^{+5.5}_{-3.5}$ |
| Weber & de Boer 2010 [105] | NFW ^b | 8.33 | $20.4^{+17.11}_{-6.4}$ | $10.8^{+3.4}_{-3.4}$ | $118.0^{+30.8}_{-15.8}$ | $4.5^{+0.4}_{-0.4}$ | $26.2^{+10.3}_{-5.5}$ |
| | NFW ^b | 8.33 | $6.32^{+1.26}_{-0.78}$ | $25.2^{+4.6}_{-4.6}$ | $95.1^{+10.1}_{-8.4}$ | $7.1^{+0.6}_{-0.6}$ | $13.4^{+2.8}_{-2.1}$ |
| | BE | 8.33 | $6.58^{+1.3}_{-1.3}$ | 10.2 | $22.0^{+3.5}_{-4.4}$ | $4.0^{+0.8}_{-0.8}$ | $5.5^{+2.4}_{-1.8}$ |
| | Moore ^c | 8.33 | $6.58^{+1.3}_{-1.3}$ | 30 | $306.3^{+60.7}_{-60.7}$ | $3.9^{+0.8}_{-0.8}$ | $77.8^{+38.5}_{-25.8}$ |
| | PISO ^d | 8.33 | $5.264^{+1.04}_{-1.04}$ | 5 | $11.4^{+2.6}_{-1.8}$ | $3.5^{+0.7}_{-0.7}$ | $3.2^{+1.7}_{-0.9}$ |
| Battaglia et al. 2005, 2006 [116, 117] ^e | NFW | 8 | 11.4 | $14.86^{+0.71}_{-0.49}$ | $95.1^{+5.3}_{-3.5}$ | $5.0^{+0.5}_{-0.3}$ | $19.0^{+2.4}_{-2.3}$ |
| | NFW | 8 | 11.4 | $16.12^{+0.44}_{-0.46}$ | $103.9^{+3.5}_{-2.6}$ | $5.8^{+0.3}_{-0.3}$ | $17.8^{+1.7}_{-1.3}$ |
| McMillan 2011 [120] | NFW | 8.29 | $8.49^{+2.85}_{-1.59}$ | $20.2^{+4.3}_{-4.3}$ | $99.5^{+11.9}_{-8.4}$ | $6.4^{+0.5}_{-0.5}$ | $15.5^{+3.2}_{-2.3}$ |
| Nesti & Salucci 2013 [122] | NFW | 8.08 ± 0.2 | $13.8^{+20.7}_{-6.6}$ | $16.1^{+12.2}_{-5.6}$ | $125.9^{+75.6}_{-26.1}$ | $7.0^{+3.5}_{-1.3}$ | $18.0^{+17.3}_{-8.5}$ |
| | BURK | 7.94 ± 0.3 | $4.13^{+4.4}_{-1.1}$ | $9.26^{+4.0}_{-3.0}$ | $22.9^{+21.4}_{-5.0}$ | $7.3^{+11.5}_{-2.1}$ | $3.2^{+5.5}_{-2.2}$ |
| Xue et al. 2008 [123] ^f | NFW ^g | 8 | $4.2^{+0.3}_{-0.3}$ | $21.9^{+1.1}_{-1.4}$ | $53.7^{+7.9}_{-6.2}$ | $3.8^{+0.7}_{-0.6}$ | $14.2^{+4.9}_{-3.6}$ |
| | NFW ^g | 8 | $4.4^{+0.2}_{-0.4}$ | $20.8^{+1.1}_{-1.0}$ | $52.8^{+7.0}_{-6.2}$ | $3.6^{+0.6}_{-0.6}$ | $14.7^{+5.1}_{-3.6}$ |
| | NFW | 8 | $0.99^{+0.76}_{-0.45}$ | $41.1^{+6.4}_{-5.8}$ | $25.5^{+12.3}_{-7.9}$ | $2.6^{+1.0}_{-0.6}$ | $9.8^{+9.4}_{-4.9}$ |
| | NFW | 8 | $0.47^{+0.32}_{-0.18}$ | $60.2^{+7.2}_{-7.2}$ | $18.5^{+8.8}_{-5.3}$ | $2.3^{+0.8}_{-0.6}$ | $8.2^{+8.0}_{-3.9}$ |

TABLE III: Overview of dark matter distributions as determined in the literature. r_* and ρ_* refer to the relevant characteristic radius and density for that particular type of profile. Where the profile was given in a different parametrization of the same profile (for example, concentration and virial mass), the values have been converted to r_* and ρ_* . The errors given are 1σ , which are naively converted from the error range given in that work if that range was not 1σ . $\Sigma_{DM,GC}^{FoV}$ (see Eq. A10) is the integral over the density of the galactic center inside the field of view of our observations, divided by the distance squared to each infinitesimal mass. $\Sigma_{DM,BS}^{FoV}$ is the same, but for the blank-sky dataset from Boyarsky et al. 2014. The errors on these projected mass densities are either 0.5σ to account for the degeneracy between the 2 parameters of the DM distribution, or 1σ if the fit from that study fixed one of those parameters (for example using a scaling relation between c and M_{vir}).

a) the two descriptions are using different baryonic disks. b) some baryonic parameters are fixed in the fits. These two NFW's are the two extremes with reasonably good fits. c) the Moore model is very cuspy by design. d) the pseudo-isothermal sphere has an almost flat profile in the center. e) the second NFW takes anisotropy into account, and is a better fit than the first. f) analysis calibrated on two different simulations. g) includes an adiabatic correction.

the field-of-view and the assumed DM particle lifetime, flux and projected mass are interchangeable in this study. This produced a range of fluxes that are in agreement with our projected mass brackets for the GC, and the flux ratios of the GC to M31, and GC to blank-sky. The confidence ranges from [113] are tighter than our literature-brackets, therefore we retain the latter in all joint analyses.

To round off this discussion about the dark matter masses, we shortly touch upon the dark matter content of Perseus and Andromeda in order to compare our observations in Figure 2 of our paper. As for the Milky Way, we compile available literature profiles of these objects and use those to determine the total dark matter mass present in the field of view of our observations [1]. This is a more straightforward calculation as the physical size of these objects is much smaller than their distance to us. We compute the enclosed projected mass of these literature profiles within the field of view (corrected for detector gaps), weighting by the exposure time of the different exposures, and then divide by the distance to the object squared to arrive at $\Sigma_{DM}^{Perseus}$ and Σ_{DM}^{M31} . For Perseus, we consider the profiles as determined by [154–159], and those by [114, 115, 118, 119, 160–162] for Andromeda.

Appendix B: Ion Abundances and Emission Lines

The Galactic Center is an object with a complicated signature in the X-rays. As [163] show, not only does the GC show multi-temperature components in the X-ray spectra, these components also vary quite dramatically spatially over the field-of-view of Chandra, which is about half as large as that of XMM-Newton. The low temperature component as measured by [163] typically has values of 0.7 – 0.9 keV, while the high temperature component can be as hot as 6 – 9 keV. The spatial variations in the elemental abundances of Si, S, Ar and Ca are reported to be as high as a factor 2 or 3, with only Fe having a reasonable

homogeneous distribution. Our integrated spectrum of the entire inner 14' of the GC therefore will be a superposition of all these components, complicating our analysis significantly.

Restricting our modelling to the cleaner parts of the spectrum, 2.8–6.0 keV, we could find a reasonable fit using a single-temperature `vvapec` component with the elemental lines added manually as gaussians, and a folded powerlaw to account for non-thermal emission. No satisfactory two-temperature fits were found for temperatures in the range given by [163], even when extending the energy range of our analysis⁴. We did not consider more than two temperature components, because it introduces too many degeneracies.

As mentioned, the emission lines from heavy ions are added by hand. We start with the strongest lines known (see Table II), and work our way down so long as the fit requires it. As mentioned, the line detected at 3.539 keV might be influenced by the Ar XVII complex at 3.685 keV and the K XVIII lines at 3.515 and 3.47 keV. To explain the 3.539 keV line with Ar XVII, the width of this line should be much larger (95 – 130 eV) than what can be expected from the instrumental response based on simulations of this Ar complex. In addition, the flux in this Ar XVII complex would be higher than that of the same ion at 3.13 keV, which should not be possible based on the atomic data in Table II.

For the K XVIII lines, it is unfortunately not possible to constrain their contribution to the 3.539 keV line in the same way as for Ar XVII, since we do not have other, stronger, detected lines of the same ion in our spectrum. In this case, one may attempt to predict the ratio of K XVIII flux to the fluxes of ions of other elements such as Ar XVII, Ca XIX, Ca XX, S XVI, etc. based on temperature and relative abundances. Since the GC emission consists of many different temperature and abundance components, it should be necessary to compute an estimate of the K XVIII flux for many different combinations of temperature and abundance. Based on the flux of each of the different detected strong lines in turn and assuming solar abundance (similarly to the analysis of Section 4 of [2]), the predictions for the K XVIII flux can vary by more than an order of magnitude. Even without considering deviations from solar abundance (which may be as large as a factor 3 [164]), the detected flux in the 3.539 keV line falls within these predictions for a respectable fraction of these physically plausible scenarios. It is therefore not possible *based on the GC data alone* to exclude the astrophysical origin of this 3.539 keV line in the GC.

⁴ The two-temperature fit can be made satisfactory e.g. by adding 1.2% systematic error in quadrature – a value much larger than the typical systematic errors for line-like uncertainties (~0.5%, see Sec. 5 of [127] for details). When adding such large errors, the `vvapec` temperatures become consistent with previous works (e.g. [163]) and the abundances of S, Ar, Ca and K are 0.8-1.2, 1.2-1.8, 1.6-2.4 and 0.3-3.4 Solar values at 68% level, respectively, in full accordance with [130].